

4
Equipment and Process Design

I. David L. Bogle and B. Eric Ydstie

Abstract

The chapter introduces the computational basis for equipment and process design in the chemical manufacturing industries. Problems, discussed through the use of case studies, range from modeling, simulation and optimization of existing, and proposed processes. These case studies include minimization of exergy losses in distillation through design and control, conceptual design of a complex, multiphase system with fluid flow from pilot plant scale-up data, handling uncertainty in the design of a multiphase reactor, a biochemical process design, and control system design for a fluid bed reactor modeled using a population balance approach. In all of these studies we focus on exploiting a very rich mathematical structure defined by conservation laws and the second law of thermodynamics. The basic objectives will be briefly outlined dealing with the fundamentals of modeling systems of considerable complexity. The hierarchical modeling approach will lead to classes of systems that are suitable for the use of optimization, control design, and the study of the interaction between these for both unit operation and flowsheet design. Design objectives continue to include profitability, but are increasingly directed towards flexibility and robustness to allow for greater attention to responsiveness to market demands, and for improved environmental performance. Controllability is also currently a focus of attention since flexibility implies dynamic performance objectives that include change of product and feedstock as markets change and environmental constraints become more important.

The work we describe in the case studies represent recent developments and trends in the industry in the area of computer-aided process engineering (CAPE). The applications focus on the use of optimization techniques for obtaining optimal designs and better approaches for controlling the processes close to or at the optimal point of operation. Designs use rigorous models based on thermodynamics, conservation laws, and accurate models of transport and fluid flow with particular emphasis on dynamic behaviour and market condition uncertainties.

Computer Aided Process and Product Engineering. Edited by Luis Puigjaner and Georges Heyen

ISBN: 3-527-30804-0

4.1 Introduction

Engineering design combines the need to specify a unit or system that can manufacture a product to meet output specifications while creatively developing new approaches with the potential to improve the performance of existing units. In many parts of the process industries this is now done routinely using computer-aided process engineering (CAPE) tools. Such tools mean that many alternative designs can be developed and evaluated and that designs can be optimized to obtain the best performance under a wide range of market conditions. Only a few years ago it was impossible to carry out such studies for all but the simplest processes. However, very significant advances have been made in optimization theory, modeling complex systems, and nonlinear control over the last decade. These new methods take advantage of the rapid increase in computational speed, distributed and Web-based computing, flexibility in software development, and graphical interfaces to a degree not imagined a few years ago. This conflux of trends of ideas will necessarily lead to opportunities to better the design of, optimize, and operate chemical processes, as we are able to analyze and integrate a much broader range of physical scales and physical phenomena with CAPE tools.

In this chapter we will outline some recent trends in equipment and process design through a series of case studies. We have chosen to focus on cases where the use of simulation tools was significantly challenged and where opportunities for new areas of application, as well as new research, are present.

When new processes are being developed there is an important requirement to obtain accurate property data on which to base the design. This means that for process development there is a strong need to tie the design process with bench and pilot plant data to attempt to reduce uncertainty. Of course, CAPE tools allow us to do this more efficiently. In several case studies this has been achieved. A second trend is the need to obtain more accuracy on spatial distributions as the production of by-products, for example toxic wastes or unsafe local transients, need to be reduced or eliminated. This can now be done with Computational Fluid Dynamics (CFD) calculations and one of the case studies uses this capability.

One of the key aspects of design is the design of objective specifications. These are needed, in the first instance, to make a product to a minimum specification and quantity at least cost. Increasingly other objectives are becoming more important such as: environmental (least waste, least water usage, least CO_2 generation), safety (least toxic by-products), flexibility (maximizing the window of operation), controllability (metrics based on closed loop responses to disturbances), and uncertainty (based on expected distributions of key variables).

4.2 The Structure of Process Models

In this section we will very briefly review the basis for process modeling, a field whose aim it is to develop the physical relationships that will allow us to make pre-

dictions, using mathematical models, of how the choice of design and control variables impact the quality and quantity of a product we make. The field of modeling, of course, is extremely broad. However, a fact that is often overlooked is that thermodynamics, most notably the second law, provides us with a very rich framework for analysis of the topological structure of vector fields that define the static and dynamic behaviour of that class of systems we are interested in discussing.

For example, classical thermodynamics defines the relationships amongst the extensive variables used to define conservation laws (conservation of energy, mass, charge, and momentum) and the intensive variables (temperature, pressure, chemical potential, voltage, and stress) that need to be controlled in order to maintain quality. Process design and control need to be concerned with both types of variables. The topological structures of these vector spaces are very different, however, and it is important to keep this fact in mind. The space of intensive variables is usually quite smooth since the intensive variables provide driving forces for flow and sharp gradients in temperature, pressure, electric field, stress, and chemical potential are difficult to maintain. The space of extensive variables can be quite irregular since the energy, composition, charge, density, etc., are discontinuous across phase boundaries. This has consequences for how we solve the conservation laws since these are stated in terms of the extensive variables. A thorough understanding of the underlying topology of the problem at hand can provide insights that can be used to obtain better solutions more rapidly, and solution structures may be obtained that are the result of discontinuous jumps in logic that are normally difficult to encapsulate in stand-alone computer programs.

All systems we deal with satisfy to very high degree of accuracy the basic axioms of equilibrium thermodynamics:

- The state of a fluid/solid element is represented by the $(n+2)$ dimensional vector $Z = (U, V, M_1, \ldots, M_n)^T$ of extensive variables. U is the internal energy, V the volume, and M_i is the amount (mass or moles) of chemical component i. This state can be augmented to include charge, momentum, and indeed any other extensive property.
- There exists a C^2 function $S(Z)$, called the *entropy*, which is first order homogeneous so that for any positive constant λ we have $S(\lambda, z) = \lambda S(z)$.
- The entropy of an isolated system increases (second law of thermodynamics).
- The energy of the system is conserved (first law of thermodynamics).
- $\partial S/\partial U > 0$ (the temperature is positive).

The vector Z of extensive variables belongs to a convex subset of $\mathbf{R}^{n+2}$, which we denote by Σ. Based on these concepts and the conservation laws derived therefrom we develop optimization and control models for almost all unit processes of chemical process systems, the structure of phase and reaction equilibrium, and the potentials (pressure, temperature, chemical potential) used to derive transport relations.

In equilibrium thermodynamics we can combine subregions of a system while retaining the idea that the extensive variables describe the state of the system. This means that two fluid elements with states Z_1 and Z_2, respectively, give a new element when combined with the state $Z_3=Z_1+Z_2$. The second law of thermodynamics can now be stated in the following manner:

$$S(Z_3) \geq S(Z_1) + S(Z_2) \tag{1}$$

In other words, the entropy of combined systems is never smaller than the sum of the entropies of its subsystems. It follows that for any positive constant λ:

$$S\big(\lambda Z_1 + (1-\lambda)Z_2\big) \geq S(\lambda Z_1) + S\big((1-\lambda)Z_2\big) \tag{2}$$

Using the homogeneity gives the relationship:

$$S\big(\lambda Z_1 + (1-\lambda)Z_2\big) \geq \lambda S(Z_1) + (1-\lambda)S(Z_2) \tag{3}$$

This expression shows that the entropy is concave. Concavity of the entropy function and dissipation by entropy production lies at the heart of the beautiful structures that emerge as we simulate the static and dynamic behavior of process systems. Consider for example phase equilibrium. When Gibbs developed the tangent plane criteria for phase stability he used concavity of the entropy as a basis for defining the condition for phase equilibrium as shown in Fig. 4.1.

The slope of the supporting hyper-plane indicated satisfies:

$$\Sigma^*(w) = \sup_{Z\in\Sigma}\big(S(Z) - w^T Z\big) \tag{4}$$

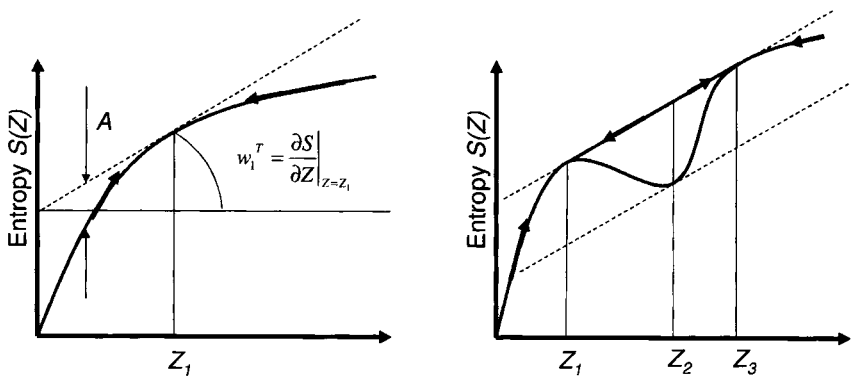

Figure 4.1 Illustration (a) shows a projection of an entropy function and a unique point of stability indicated at the point Z_1. The slope of the tangent line, w_1 defines the intensive variables at that point. Illustration (b) shows a projection, as it might arise in a cubic equation of state like the van der Waals equation. In this case the EOS gives three points where the slope, and hence the intensive variables, are the same. The actual entropy is defined to be the smallest concave envelope as indicated by the straight line segment. Along such segments the entropy is concave but not strictly concave. Entropy functions below the line are in violation of the second law.

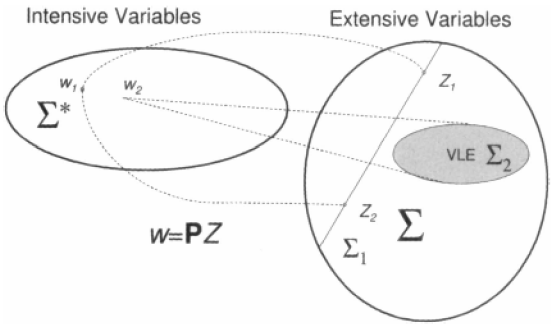

Figure 4.2 The mapping $w = PZ$ from the space of extensive to the space of intensive variables is not one to one. The line Σ_1, corresponding to a uniform scaling of all extensive variables maps to the same point w_1 in Σ^* indicating that pressure, temperature and chemical potential remain invariant. Subregions with positive measure (regions in Σ with phase or reaction equilibriumΣ) map to points with zero measure (in Σ^*).

The vector w is called the vector of intensive variables in the entropy formulation. These variables belong to the convex set:

$$\Sigma^*(w) = \sup_{Z \in \Sigma} \left(S(Z) - w^T Z \right) \tag{5}$$

The sets Σ and Σ^* are subsets of $\mathbf{R}^{n+2}$ and they are dual in sense of Legendre-Fenchel.

It is critical to note that the mapping between these spaces is not one to one. The lack of invertibility between *extensive* and *intensive* parameters occurs on the subsets of Σ where the entropy, although concave, is not strictly concave as illustrated in Fig. 4.2. If the entropy is linear it follows that it is merely concave in some directions. Along these directions we can scale the extensive variables without changing the intensive variables. We may also have discontinuities in the space of extensive variables (Callen 1985).

The noninvertibility between the space of extensive and intensive variables is critical for process design. It allows the scaling of the size of the system along lines in the space of extensive variables without changing the intensive variables. We can therefore independently control the "size of the systems" (amount present in each phase) without changing the quality (pressure, temperature, chemical potential). In more practical terms, we can also change the hold-up without changing the properties of phase or reaction equilibrium. These scale invariant properties are so common that we use them always without thinking in thermodynamics.

In transport we find similar scaling laws centered on the ideas of dimensionless numbers like the Reynolds, Rayleigh, Nusselt, and Damkohler numbers. These numbers include transport properties and estimates of the size of the domains. The relationship between size and shape, being the extensive properties that define the domain of interest, and the intensive properties is much more complex. It is especially difficult to unravel in systems that integrate fluid flow, chemical reactions and multiple phases.

In chemical engineering we need to develop models to deal with systems that are not at equilibrium and have variations in space and in time. By far the most common approach is to develop a lumped description (a network model) of the process. In this

approach we use nodes distributed in space that are interconnected by steady or unsteady flow of material and energy. These nodes may represent a single phase in a separation system, a unit process, or an entire plant. Irrespective of size we have additivity satisfied so that we can write conservation equations:

$$\frac{\mathrm{d}}{\mathrm{d}t}\text{inventory} = \text{inlets} - \text{outlets} + \text{generation} \tag{6}$$

Inventory is a macroscopic measure of the total internal energy, volume, number of moles of each species respectively so that

$$v^T = \left(U_t, V_t, M_{1t}, \ldots, M_{nt}\right) \tag{7}$$

where the subscript t refers to total. The balances can be written on the form:

$$\frac{\mathrm{d}v}{\mathrm{d}t} = \underbrace{\phi(x, m, d)}_{\text{Netflow to system}} + \underbrace{p(x, m, d)}_{\text{Net Generation}} \tag{8}$$

The variables x, m, d represent the state, manipulated and disturbance variables needed to define the flow and generation variables. We make a distinction between the extensive variables Z and the inventories v. The extensive variables were assumed to represent the state of the system with some degree of accuracy. The inventory v *does not* represent the state unless the system under consideration is spatially uniform in each phase.

For example, consider a distillation column with benzene as one component. The macroscopic inventory balance can be applied to the entire system with generation equal to 0. But the inventory of benzene does not represent the state of the system since it can be distributed in an infinite number of different ways throughout the column. In order to have a unique (state) description we need to look at a more refined system. In a stage to stage model of the system we find that the inventory in fact represents the state to a good degree of approximation.

Thus we find that uniformity can be approached asymptotically by tessellating the physical space finer and finer. In the limit we define the point densities:

$$\rho = \lim_{V\to 0}\frac{M}{V}, \quad \text{and} \quad z = \lim_{M\to 0}\frac{Z}{M} \tag{9}$$

where $M = \sum_{i=1}^{n} M_i$ is the total mass or moles. These limits exist if the spatial variations of $Z(x)$ are sufficiently regular. Local pressure, temperature and chemical potential is defined as before.[1] The inventory v_i is related to the density of the extensive variables z according to:

$$v_i(t) = \int_V \rho z_i \,\mathrm{d}V \tag{10}$$

1 This Assumption is called "the principle of local action" or *the hypothesis of local equilibrium*. The latter term can be misleading since it does not at all mean that the TRP system is at equilibrium: there may be variations is space and time.

And for a system with one spatial dimension partial differential equations of the form:

$$\frac{\partial \rho z}{\partial t} + \frac{\partial f}{\partial x} = \sigma \tag{11}$$

t is the time, x is position, pz defines the local state vector, $f = (f_{1,\ldots,}f_{n+2)}{}^{T}$ is the transport velocity and σ refers to the production rate of property z. These equations are easy in principle to extend to include the momentum transfer and the equations then include the Navier-Stokes equations as a special case.

By applying the ideas above to the entropy we find that we can write the entropy balance of the form

$$\frac{\partial \rho s}{\partial t} + \frac{\partial f_s}{\partial x} = \sigma_s \quad \text{where } \sigma_s \geq 0 \tag{12}$$

where s is the entropy density, f_s represents the entropy flux through a point and σ_s is the entropy production. The inequality states that the production of entropy is always positive. In a nonequilibrium system the rate of entropy production represents the dissipated energy and an important design objective therefore is the minimization of entropy production. In irreversible thermodynamics the entropy production is given by the expression

$$\sigma_s = X^T L X \tag{13}$$

where the vector X represents the thermodynamic driving forces (these are gradients in pressure, temperature and chemical potential) and L is a positive definite matrix. It is quite straightforward to show that the entropy production is minimized when the forces are kept constant and equal in certain staged systems (Farschman et al. 1998). This leads to the important idea of equipartition of forces as a criterion for energy efficient process design (Sauar et al. 1996).

The assumptions made up to this point are well tested and hold at very small scales and sharp gradients. Only at extremely small scales and extreme gradients is it necessary to resort to other techniques like lattice Boltzmann methods to give better approximations to physical behaviors.

The field of process control has typically concerned itself with how to adjust the flows in a network with fixed network topology. The field of process design has typically been concerned with how to design the network topology. The distinction between the two fields is becoming more and more artificial however since the topology and flows are very closely interlinked. In a high performance system it is not possible to separate the two and equipment and process design should be considered in conjunction with the process control.

4.3
Model Development

The book by Hangos and Cameron (2001) sets out systematic approaches to model development and analysis breaking down the steps as shown in Fig. 4.3. If undertaking a first principles modeling task, it is important first to establish the need for the model which define the "goalset definition" in their methodology. These should be specific and quantifiable and a list of common objectives is listed in the first section of this chapter. Models for controllability for example will be different from those required for capital cost minimization.

As outlined in the previous section conservation relations can be developed for mass, component mass, energy, momentum, or population of a species. The choice of which relations are required will depend on the nature of the system. For example the population balance relations are only required if there are discrete elements whose properties affect the purpose of the system being analyzed. These may be solid particles, or micro-organisms, or bubbles in liquid or vapour phase. Further constitutive relations will be required to model transfer rates, reaction rates, property relations, and equipment and control constraints, as appropriate.

Increasingly there is a need in process development and design to develop more detailed models of parts of the process. This is done for a variety of reasons. More confidence may be required in a new design of unit operation, particularly if the unit has only been used in the prototype. Dynamic simulation requires a more detailed model of complex units so that time-dependent elements, especially those where the time delays are related to transport effects, can be predicted with some degree of accuracy. Contractors are increasingly being required to provide dynamic simulations with the final delivery of a process design. Safety and environmental expectations of customers and local residents now can require more detailed models of plant items. All of these require sophisticated models.

4.4
Computer-aided Process Modeling and Design Tools

Most modeling and design is now done using CAPE tools. Bogle and Cameron (2002) recently reviewed the tools available and how they are used throughout the design and development lifecycle. Sequential modular packages commonly used in industry are based on calculating the sequence of unit operations in the order in which they appear in the flowsheet, using modules for each unit of the flowsheet. If the flowsheet contains one or more recycles a stream must be guessed ("torn") and iterative methods are used to converge the calculated values to the guessed values. Most modules are written in FORTRAN, a high-level computer language widely used in the engineering and technical world. Examples are AspenPlus and ProII. The calculation procedure is at the heart of the computational procedure used by these packages to solve the problem. However, there are many other parts which make the whole package a convenient tool for the design engineer. The following are

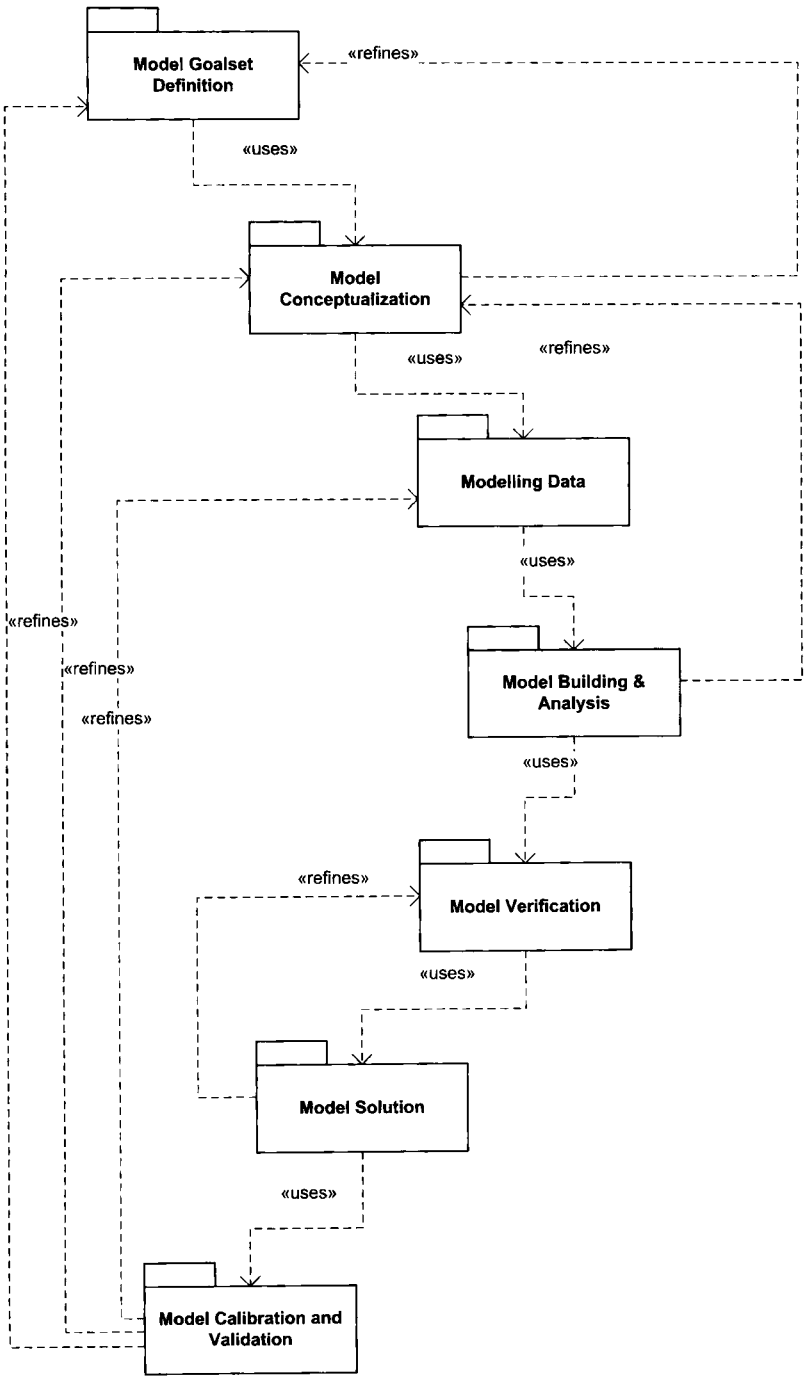

Figure 4.3 The systematic approach to model building (Hangos and Cameron 2001).

the most common elements: input interpreter, unit operation subroutines, physical property prediction subroutines, algorithms to select torn stream, recycle convergence block, costing databank, output post-processor.

Equation-oriented packages use a matrix representation of material and energy balance problems. The set of modeling equations is assembled and can be solved numerically. From the equation set an occurrence matrix is assembled. This dictates the number of degrees of freedom, which in turn dictates the number of specifications that can be made. Once a square system is obtained the design equations can be solved giving the solution to the design problem. gPROMS (Oh and Pantelides 1994) and Aspen Custom Modeler are the most prominent examples currently. These systems have advantages over modular systems in that it is easier to set up and solve other types of problems such as dynamic simulation, optimization, and parameter estimation.

In both cases models of each unit operation are required. In the design tools simple models are usually used so that overall designs for process flowsheets can be assembled quickly to be used as targets for more detailed design of individual units. There are many software programs for doing detailed design calculations obtaining internal flows and configurations such as the number of trays in a column or the size of a reactor's packed bed. These calculations are often done using specialist programs which require a more detailed level of modeling. Eggersmann et al. (2002) reviewed the current state of such programs.

Network representations use diagrams and pictures and show in a graphical manner the topological properties of a system as they are distributed in space and/or time. Examples of systems that can be effectively represented as networks include a flowsheet of a chemical process, chemical reaction networks, metabolic pathways, decision trees and transportation systems. An example of such a network is shown in Fig. 4.4 on the left. Each node represents an activity where information/material is processed, whereas each vertex can represent flow of information, material or energy. We note that several activities can be lumped together as indicated by activity A_4. We can therefore decompose a process into a multiscale hierarchy ranging from the molecular to the macrolayer where economic decision making takes place (Grossman and Westerberg 2000; Ingram et al. 2004). These decompositions have motivated very active research which very recently has led to significant breakthroughs in our ability to model very complex systems with integrated fluid flow, multiple phases and population balances to express the dependency of physical properties on particulate matter. It is important to note that the additivity of the extensive variables allows us to combine such nodes very easily and we therefore have computational architectures with integrating scaling (Farschman et al. 1998; Mangold et al. 2002). These architectures are flexible and amenable to parallel computing using highly distributed Web-based systems and or cluster computer. Such systems are becoming increasingly easy to define and maintain due to interface standards like TCP/IP and CAPE-OPEN (www.colan.org).

In this paper a series of case studies is presented where a sophisticated level of modeling was required. This required the use of commercial tools but enhanced with detailed models of the units that were not routinely available in the design sys-

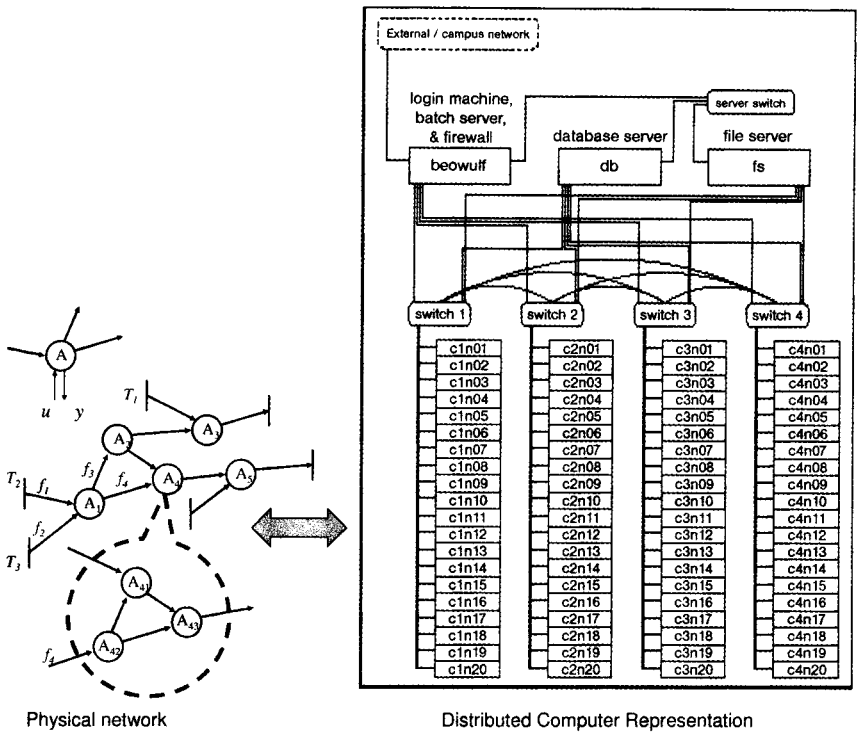

Figure 4.4 The topology of the process system can be mapped onto a distributed cluster of fast computers interconnected by a high bandwidth communication for parallel processing.

tems on the market. This trend seems set to expand – that customers will require high-fidelity models of critical units often integrated into the design systems that they currently use so that the systems can be used for troubleshooting, startup and shutdown, and for plant enhancements. A closer relationship is required with existing plant, pilot plant, and bench-scale experimental data to improve the fidelity of the models. A rigorous thermodynamic basis is also necessary. This constitutes a development from the use of design systems as balance tools setting targets for detailed design to a staged use of the tools with increasingly sophisticated models used to achieve different objectives. These case studies highlight these more challenging objectives.

4.5 Introduction to the Case Studies

In the following sections we give an overview of five case studies that describe how CAPE tools have been used to improve process design and control for existing and conceptual processes. The first two case studies, of distillation and of a complex mul-

tiphase reactor, involve detailed and thermodynamically rigorous models, which are used to ensure the design will meet the productivity targets and reduce or minimize the energy consumption and hence improve the environmental performance. The third case study also considers a multiphase reactor and shows how uncertainty can be systematically considered in the design of the unit. The final two case studies, of a biochemical reactor and separation system and of a fluidized bed reactor, both involve particulates, which requires the use of population balance techniques to model the fluid particle systems. Each case represents a unique challenge and opportunity for modeling and optimization.

4.5.1 Case Study 1: A Binary Separation Case Study

Distillation column design is a well established activity where the use of CAPE tools is routine. However design is usually based around well established procedures that are now being challenged with increasing need for design for environmental performance or for better closed loop performance. The CAPE tools allow engineers much more scope for developing designs to meet these new objectives. In this case study a column for the separation of vinyl chloride monomer was designed to meet environmental targets and determining the effect on closed loop dynamic behavior. While the conventional wisdom is that optimizing environmental performance results in a degradation of performance by other measures, this case study shows that is not necessarily the case.

For this design a column with total condenser and reboiler was required for the purification of vinyl chloride monomer (VCM). The product quality is fixed at both ends of the column which in turn fixes the product withdrawal at both ends of the column. The feed location is an independent variable and was to be optimized. For binary mixtures there will be one feed plate where the feed stream and the internal column flowrates match. For an optimized column the feed always enters the column on a single plate and is not split over a range of plates. The pressure drop between the top plate and the reboiler is approximately 0.165 bar and depends on the number of plates and the size of the internal flow rates. The objective was to develop a column design which utilized the energy most efficiently by trying to avoid irreversible losses. A diabatic distillation column is a column with intermediate side-heating and cooling on individual plates. Parts of the heating and cooling utilities are re-directed from the bottom reboiler and the top condenser of the adiabatic column to individual plates, generally around the feed plate. The advantage of such a configuration is that heating and cooling can be supplied at alternative temperature levels and the column profiles can be moved towards the reversible column profiles, as discussed by Kaibel et al. (1989, 1990). An operating curve close and parallel to the equilibrium line is a thermally optimal column configuration.

4.5.1.1

An Environmental Design Problem: Minimizing Exergy Loss

The concept of equipartition of the driving forces as an optimization criterion to minimize the exergy losses was first introduced by Ratkje et al. (1995). Earlier, Tondeur and Kvaalen (1987) proposed the equipartition of the entropy production (EDF) criterion while Sauar et al. (1996) showed that a better approach was to design for uniform driving forces for different paths over a given transfer area will yield minimum entropy production. The criterion has been further discussed by Kjelstrup et al. (1996) and Sauar et al. (1997). Similar techniques based on thermodynamics have also been used to find the optimal temperature profile in equilibrium chemical reactors (Sauar and Ydstie 1999).

The method used here is to directly optimize the exergy losses to minimize the production of entropy, the ExL criterion. Entropy is produced because of the existence of driving forces. To make uniform these driving forces the separation exergy has to be redistributed and this should be an automatic result of minimizing exergy loss. The advantage of the ExL criterion over the EDF criterion is that it considers all possible sources of entropy production without the need for additional constraints.

Kaibel (1990) pointed out that the main exergy losses occur on the feed plate due to (1) the feed condition and the adiabatic column design and (2) due to heat transfer, and pressure losses and are necessary because of there being a finite number of plates. The latter (2) can only be reduced by substantial capital investment. The first (1) can be improved by minimal capital investment, i.e., specifying the feed condition correctly and a re-distribution of the heating and cooling utilities. Hence, the degrees of freedom are the heating/cooling utilities on each plate, the feed location, and the feed condition. The feed location and composition have been determined by traditional means.

Heating and cooling requirements were calculated for exergy optimized 23, 25, and 35-plate VCM columns (Table 4.1). For the 25-plate column, seven side-reboilers and two side-coolers (Hagemann et al. 2001) would be required to minimize exergy

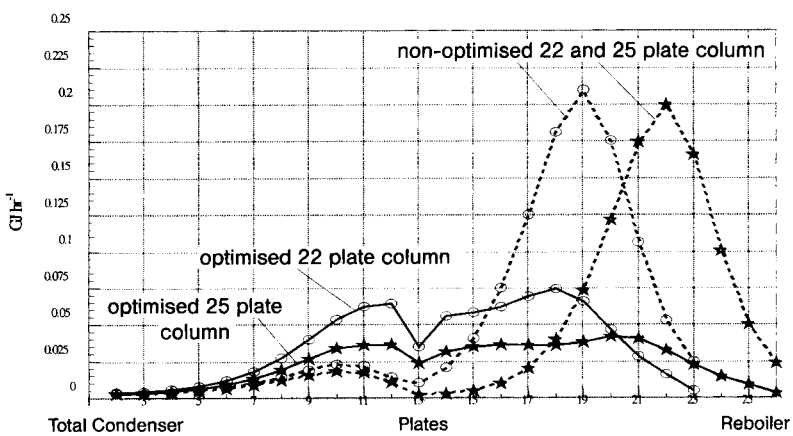

Figure 4.5 Exergy loss profiles for the VCM column (ExL Criterion).

Table 4.1 Exergy comparison of the diabatic with the adiabatic column [GJ h^{-1}].

Adiabatic – Diabatic	22 Plates	25 Plates	35 Plates
Difference in total cooling duty	−0.285 (+31.6%)	−0.182 (+20.7%)	−0.123 (+14.9%)
Difference in total heating duty	−0.341 (−9.8%)	−0.385 (−11.5%)	−0.34 (−10.8%)
Difference in total exergy losses, including losses due to intermediate heating or cooling	−0.552 (−25.1%)	−0.684 (−37.3%)	−0.592 (−35.4%)

loss. Seven reboilers is not a practical option but we will see later how much of this benefit can be achieved by a more practical solution. The exergy loss profiles of the VCM column are shown in Fig. 4.5. The profiles for the nonoptimized adiabatic column show very large exergy losses within the stripping section caused by large vapor phase gradients. In contrast, the optimized column shows an almost uniform profile over the mid section of the column. This is directly related to the re-location of heating and cooling utilities. The overall exergy losses are substantially lower for the optimized column and decrease further with an increase in the number of plates. A dip in the exergy losses at the feed plate can be explained with the composition of the entering feed flow rates. The flow rates (vapor + liquid) closely match the outlet feed plate compositions and, hence, do not create exergy losses.

4.5.1.2

A Practical Interpretation

For the 25-plate column in Table 4.1 the thermally optimal design requires side-heating utilities on plates 14 to 20 and side-cooling on plates 12 and 13. For industrial application an additional seven side-heating units and two cooling units is clearly not a practical solution. However the intermediate cooling utilities can be neglected as these represent only 5.7% of the total required cooling utilities and the seven side-heating units can be replaced by one side-reboiler with very little effect on the results. This single side reboiler, located on plate 15, provides 74% of the side-reboiler utilities of the diabatic thermally optimal design, with an increase in exergy losses of only 11%. This side reboiler is located in an area of low driving forces.

Figure 4.6 shows the temperature profiles for the adiabatic, diabatic thermally optimal, and diabatic one side-reboiler VCM column design. For the diabatic thermally optimal column design, the temperature and concentration (not shown) profiles are almost linear between the pinch points at both ends of the column. For the diabatic column with one side-reboiler the profiles are also closer to being linear than for the adiabatic design. The critical factors for obtaining such "near linear" profiles are the location and size of the side-reboiler as well as the condition and location of the feed stream. A shifting of the side-reboiler into a region of already high-driving forces, or using the side-reboiler to dump available heating utilities, will increase the exergy

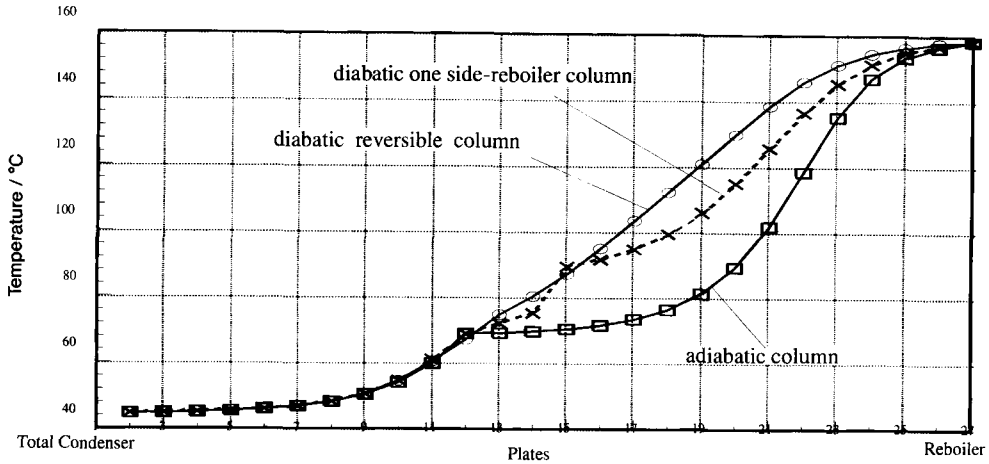

Figure 4.6 Temperature profiles for adiabatic and optimized 25-plate column.

losses but, perhaps more importantly for the control system design, will alter the column profiles away from near linear profiles.

This optimized column design with one side-reboiler column configuration has been used to study a possible control system design and compare it with an adiabatic 25-plate VCM column configuration.

4.5.1.3

Effects on the Controllability of the Process

The new process design has a different dynamic response to feed disturbances which in turn can provide equivalent process stability and/or less capital investment. The design for both columns is based on the widely used LV column control configuration (Luyben 1990). The operating objectives for the VCM column are high product recovery and product purity. The selection of the LV configuration has the advantage that it has a direct effect on the product compositions and is weakly dependent on the level control scheme (Skogestad 1997). The controllers were tuned using the Zeigler-Nichols tuning method.

Results for 3% feed flow rate and 3 % feed composition disturbances and for a 1 °C feed temperature disturbance are tabulated in Table 4.2. The response time, defined as time taken for the output variable to return within a fixed distance from the new or old stationary value, has been used as a measure of the quality and stability of the process and control system design. Table 4.2 gives a summary of the response times, in hours, after the feed disturbances at time 0.05 h. It is assumed that the product compositions have reached a new stationary operating condition if the differential values are within (and remain within) ±10% of their final values. The results show that especially for the bottom composition the response times of the diabatic column are much shorter. In all of the feed disturbances reported here, except one, the dia-

Table 4.2 Summary of response times after the feed step disturbances.

Distillate Temperature (Composition) Control		
Disturbance at time 0.05 [h]	**Response time [h]**	
	Adiabatic	**Diabatic**
Flow rate: [+3.0%]	0.68	0.53
VCM composition: [+3.0%]	0.72	0.81
Temperature: [+1.0 °C]	0.69	0.54
Bottom temperature (composition) control		
Disturbance at time 0.05 [h]	**Response time [h]**	
	Adiabatic	**Diabatic**
Flow rate [+3.0%]	>0.95	0.37
VCM composition: [+3.0%]	>0.95	0.58
Temperature: [+1.0 (C]	>0.95	0.56

batic column shows better disturbance rejection. The exception is the VCM composition of the distillate after a 3.0% VCM feed composition increase. The reason for this result is the fixed side-reboiler duty. Most of the additional VCM entering the column is vapor. Hence, after the disturbance the side-reboiler evaporates a higher fraction of ethylene dichloride (EDC) until the main reboiler is adjusted to the new operating condition.

These results are perhaps surprising because the side-reboiler for the diabatic design introduces strong cross-coupling effects causing considerable oscillations within the column. However the improved controlled response is due to the removal of the sharp nonlinearity in the temperature profile (Fig. 4.6). Shifts in the internal temperature, used as a measured variable in the control scheme, are less drastic producing a more even closed loop response.

This design study was undertaken using a tray to tray column model with rigorous thermodynamics using SPEEDUP, now a part of the Aspen Custom Modeler system. The ability to develop a rigorous model was essential here in order to achieve the two goals, that of improving environmental performance and analyzing the controllability. Ideally the ability to make structural changes to the process, in this case by adding and removing side-heaters and coolers, could be done automatically but this challenge still remains. The use of integer programming techniques would permit this but they are not yet available in modeling systems.

4.5.2
Case Study 2: Conceptual Design of Multiphase Reactor

In this case study we review very briefly a challenging program for developing a new process for producing primary aluminum (Johansen et al. 2000; Johansen and Aune 2002). The aim of this joint research program amongst ALCOA, ELKEM and Carnegie Mellon is to develop a process for production of primary aluminum which reduces capital, energy and environmental costs relative to the Hall process with a significant amount (Motzfeldt et al. 1989). The process under consideration, carbothermic reduction, uses electric heating, but a carbothermic process is more energy efficient and has very high volumetric productivity leading to better economies of scale.

4.5.2.1
Carbothermic Reactor Modeling

Carbothermic reduction can be realized in a two-stage process with additional steps needed to purify the product, recover aluminum from off-gases, and recover heat. A diagram of the process is shown in Fig. 4.7 and it is based on a reversible, multiphase and multispecies chemical reaction phenomenon. The kinetics of the reaction mechanism has not been completely finalized, but ionic species identification has been conducted and there is a reaction rate model proposed by Frank et al. (1989); the reactants are aluminum oxide (Al_2O_3) and carbon (C), key reaction intermediates are aluminum suboxide (Al_2O) and aluminum carbide (Al_4C_3), and the end products are molten aluminum (Al) and carbon monoxide (CO). The complexity is illustrated by this simultaneous coexistence of solids and gases in the multicomponent reactive slag.

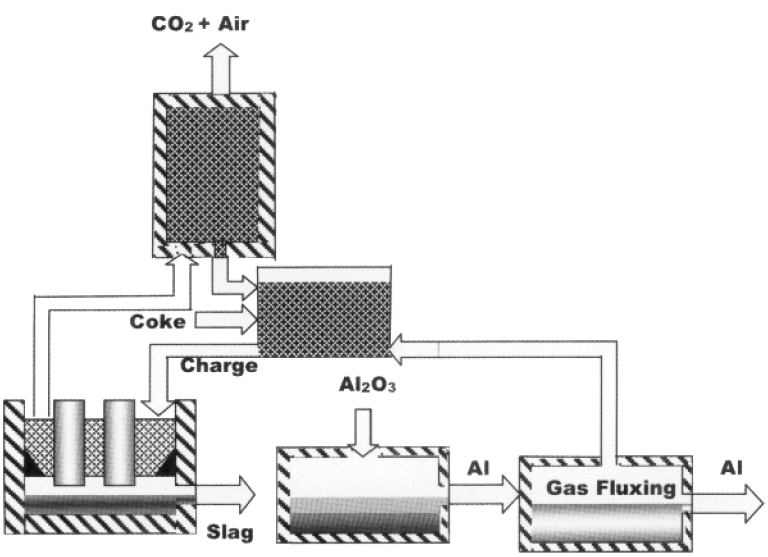

Figure 4.7 Diagram of the carbothermic aluminum process.

1. The first stage is the *pre-reduction smelting zone*. Carbon and aluminum oxide pellets are continuously fed to a submerged arc smelter, melt, react and form a molten slag contained in an inert-atmosphere, oil-cooled reactor. The reaction of aluminum oxide with excess of carbon to form the Al_4C_3-rich slag of the first stage is ($T > 1900_{(g)}$)

$$2\,Al_2O_{3(s)} + 9\,C_{(s)} \rightarrow (Al_4C_3 + Al_2O_3)_{(slag)} + 6\,CO_{(g)} \tag{14}$$

2. The second stage is the *high-temperature reaction zone*: the first-stage molten slag flows into this core stage (a multielectrode, high-temperature submerged arc reactor); the slag is heated to a higher temperature, avoiding severe local surface superheating caused in open arc reactors. Liquid Al droplets and CO bubbles are rapidly generated, with concurrent Al_4C_3 injection to avoid carbon depletion. The decomposition of the first-stage, Al_4C_3-rich slag to form the second-stage, Al-rich phase is ($T > 2000°C$):

$$(Al_4C_3 + Al_2O_3)_{(slag)} \rightarrow (6\,Al + Al_4C_3)_{(metal)} + 3\,CO_{(g)} \tag{15}$$

3. The third stage is a *vapor recovery reactor* (VRR), where Al and Al_2O vapors react with C to form Al_4C_3. Vaporization occurs as CO vapors sweep the second stage: unless $Al_{(g)}$ is recovered counter-current to incoming solid feed, metal losses are catastrophic for process economics. Undesirable vaporization is thus reduced by staging and feeding the first and second stage gas streams to the VRR. The recovered Al_4C_3 (recycle stream) is re-injected into the reactor, minimizing Al emissions and maximizing yield. Counter-current flow exceeds incoming reactant preheating needs, thus allowing for energy recovery via cogeneration.

4. The fourth stage of the process is the *purification zone*: liquid aluminum flows through an overflow weir to a flotation and skimming unit, where entrained $Al_4C_{3(s)}$ dissolved $C_{(s)}$ can be removed via proprietary technology.

The goal of our research is to develop models for preliminary design, pilot plant scale-up, optimization of the process and process control.

To make best use of energy aluminum vapors and their energy content must be recovered, preferably as aluminum carbide in the VRR. The approach we investigate solves the problem by feeding a carbon material at the top of the counter-current VRR. The carbon reacts with the aluminum compounds in a series of heterogeneous noncatalytic reactions forming solid and gas products. Liquid products, like molten slag, can be avoided by running the VRR at high temperature. The most important products are aluminum carbide, which is needed in the smelting stage of the aluminum process, and hot carbon monoxide gas, which can be used for co-generation of electricity. Garcia-Osorio and Ydstie (2004) developed an unsteady state reactor model which incorporated a shrinking core, mass transfer limited reaction separate mass and energy balances for the vapor, liquid and solid phases and dynamics distributed in space and time. The model equations take the form of conservation equations. The Al_20 and Al reactants take the form:

$$\varepsilon_B \frac{\partial c_i}{\partial t} + v_g \frac{\partial c_i}{\partial z} - D_{\text{ebi}} \frac{\partial^2 c_i}{\partial z^2} = \sigma_i + \frac{\sum_j \varepsilon_j \nu_{ij}}{V_T} \tag{16}$$

$i = Al_2O, Al$

Similar expressions were developed for the product species. Mass transfer limited diffusion was assumed for the solid gas reactions. All liquid phase reactions were assumed to be in equilibrium. The final model was solved using the method of lines and a stiff (index 1) DAE solver was used to solve the final large-scale system of differential algebraic equations. The model was matched to small-scale experiments and interfaced with proprietary thermodynamics describing the Al-O-C system for temperatures in the range 800 to 2050°C. It was found that the model predicted pilot plant results within 10% and that it could be effectively used for sensitivity studies and scale-up. An example of a sensitivity study is reported in Table 4.3. F_c is the dimensionless feedrate of carbon with the range [50–100%].

Table 4.3 Recovery and solid conversion for recovery column.

F_C*	Al_2O %	Al %	X_T %
0.5	96	16	59
0.7	98	33	43
1	98	47	32

Gerogiorgis (2002, 2003a,b) developed a number of different CFD models to study design of the aluminum producing stage (stage 2). The objective was to solve the steady state PDE problems for the potential (V), field intensity (E), temperature (T), velocity (U_x, U_y) and pressure (P) to obtain reliable starting points so as to solve molar balances for species concentration profiles in a complete model, reliable for performance evaluation. Constant thermophysical properties were assumed in many studies, although a temperature-dependent electric conductivity has been used to illustrate the strong coupling between the charge balance and the Joule heat generation term. The k-ε standard model of turbulence was used in the momentum balance in order to analyze the turbulent slag flow in the reactor. We also developed a two phase flow model to study how the gas generation impacts the fluid flow and mixing characteristics.

The finite element CFD model of the reactor has been solved for different geometries with quadratic finite element basis functions on a fine unstructured triangular grid (12,124 elements), using commercial simulation software (FEMLAB v. 2.3). Different FEMLAB multiphysics modules have been used and integrated for the simulations (Conductive Media DC, Convection and Conduction, k-ε turbulence model and a two-phase model based on constant relative slip velocity). For the present case, nominal Reynolds numbers indicate slag flow well within the turbulent regime (Re ~30,000). The steady state CFD problem with turbulence considers three PDE balances and the corresponding partial differential equations on a two-dimensional domain. The first part is the steady state electric charge balance:

$$\nabla^2 V = V_{xx} + V_{yy} = 0 \tag{17}$$

The second part is the steady state heat balance:

$$\nabla \cdot \left(k\nabla T - \rho C_p T\mathbf{U}\right) + \sigma(\nabla V)^2 - k_0 \exp\left(\frac{-\Delta G}{RT}\right)\Delta H = 0 \tag{18}$$

The third part is the steady state momentum balance, which comprises the continuity and velocity PDE system:

$$\nabla \cdot \mathbf{U} = 0$$

$$\rho(\mathbf{U} \cdot \nabla \mathbf{U}) - \nabla \cdot \left[\left(\mu + \rho\frac{C_\mu}{\sigma_k}\frac{k^2}{\varepsilon}\right) \cdot \left(\nabla \mathbf{U} + (\nabla \mathbf{U})^T\right)\right] = -\nabla P \tag{20}$$

complemented with the two standard k-ε turbulence model:

$$\rho(\mathbf{U} \cdot \nabla k) - \nabla \cdot \left[\left(\mu + \rho\frac{C_\mu}{\sigma_k}\frac{k^2}{\varepsilon}\right)\nabla k\right] = \rho C_\mu \frac{k^2}{\varepsilon}\left(\nabla \mathbf{U} + (\nabla \mathbf{U})^T\right)^2 - \rho\varepsilon \tag{20}$$

The imposed voltage on all electrode tips (V_i, $i = 1{-}6$) is set, zero voltage is used on both long horizontal domain sides to approximate the potential in the third lateral dimension, and zero gradient ($\nabla V = 0$) is used on all other wall sides to account for the insulating behavior of solidified slag. Inlet slag (2173 K) and wall (473 K) temperatures are set, and insulation ($\nabla T = 0$) is assumed at all six electrode tips. An inlet vertical slag velocity is assumed ($U_0 = 0.01$ m s^{-1}, with a suitable wall function (Gerogiorgis and Ydstie 2003a) on the walls and all six tips. A slip boundary condition is used for the slag-free surface and zero pressure has been assumed at the reactor outlet. A typical result for a two-dimensional simulation showing constant velocity contours is shown in Figs. 4.8 and 4.9.

The simulation revealed several important aspects about the process that play a role in understanding the underlying physics and impact design and scale-up. The simulation showed that short, submerged electrodes were preferable to long ones in order to get better energy distribution and flexibility for controlling the process by

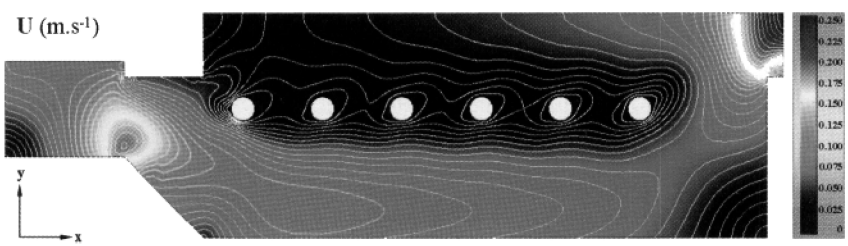

Figure 4.8 Single-phase flow model with constant velocity contours for steady state multiphysics CFD model. The slag moves under the electrodes and avoids the primary reaction zone. This problem can be solved by raising the floor of the reactor.

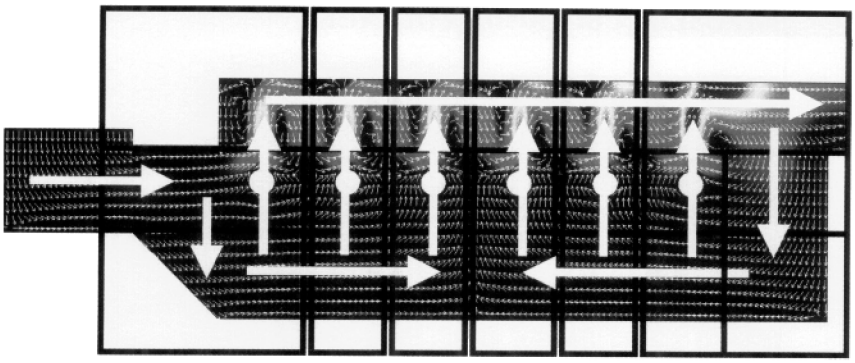

Figure 4.9 Two-phase flow model with major flows superimposed on small-scale movements leading to coarser scale representation of the system, with each zone being represented by a uniform mixing tank with inter-stage flow.

moving the electrodes. Our current studies focus on three-dimensional multiphase simulation to study the issues of back-mixing between stage 1 and 2 and the feasibility of controlling the flow between the stages.

4.5.2.2

MINLP Model for Electrode Heating System Design

One design challenge is to optimize electrode positions and the imposed voltage profile so as to achieve the reaction advance without unnecessary reactor space or energy use. Obviously, dense electrode placement and high voltage result in excessive superheating, causing aluminum evaporation, major yield reduction and losses, while sparse electrode placement and low voltage fail to achieve adequate slag heating resulting in limited conversion and low productivity. In order to address some of these issues Gerogiorgis and Ydstie (2003b) developed a Mixed Integer Nonlinear Programming (MINLP) finite volume model of stage 2. The goal here is to perform electrode placement as well as imposed voltage profile optimization for maximization of Al production under mass, heat and molar species balance constraints. The mathematical formulation is based on a CSTR series steady state process model; each finite volume is assumed a CSTR with perfect separation of reactants and products. The advance of the reversible reduction towards Al (liquid) and CO (gas) is considered governed by the overall reaction proposed in a recent kinetic study (Frank et al. 1989). A typical result from the optimization procedure is shown in Fig. 4.10.

The long term objective of the research is to develop a multiscale hierarchy of models of the aluminum process, which can be used for pilot plant design, scale-up and optimization of the final process, including control studies. Towards this end we have developed a new approach for Web-based distributed simulation (Garcia-Osorio and Ydstie 2003), which will allow the solution of modules in a network representation of the process over the web.

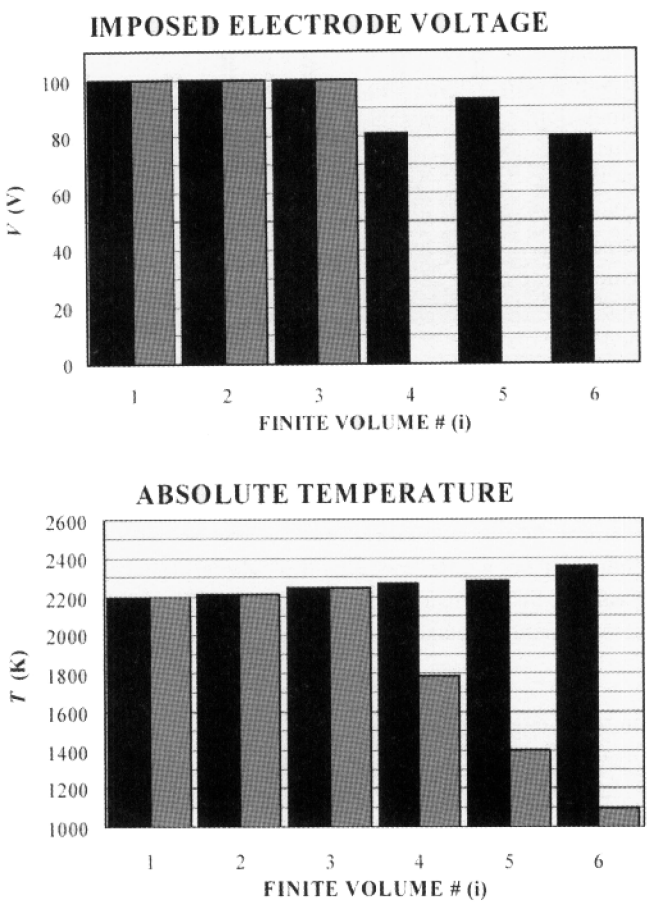

Figure 4.10 MINLP model comparing a reactor with three electrodes (gray) and one with six electrodes. The optimal imposed voltage is shown on the left while the resulting temperature profile is shown in the figure on the right.

4.5.3
Case Study 3: Uncertainty Analysis in a Multiphase Reactor

Risk analysis methods for the quantification of uncertainty and identification and ranking of major contributors can be integrated as part of the design process using CAPE tools. The risk analysis problem is a stochastic optimization of process performance under uncertainty and tolerance to operating policy variable error. This case study shows how this is applied to a multiphase reaction process where there is considerable uncertainty in the parameters. The use of stochastic optimization using complex models is a very computationally demanding problem but is now achievable on the desktop.

The general problem for design under uncertainty was stated by Swaney and Grossmann (1985) and has been solved by determining the largest possible operating window based on conservative assumptions or using scenario-based approaches. The flexibility analysis assumes a "wait and see" approach where it is assumed that operating variables can be used to achieve any possible scenario. This requires a two-stage optimization. The "here and now" approach takes design and operating variables together in a single optimization.

A design was required for the production of a pharmaceutical intermediate, formed from the amination of a bromopropyl compound produced in an exothermic multiphase reactor. Sano et al. (1998) developed a kinetic model based on reaction calorimetry data obtained under laboratory conditions in order to determine the optimum feasible and safe operating policy.

Solid particles of the active pharmaceutical ingredient (API) bromopropyl feed compound (A) reside in an organic solvent (methanol) inside the reaction vessel. A fixed volume of a 50 wt% aqueous dimethylamine reagent (B) is added to the vessel at a constant flow rate under continuous agitation. The solids gradually dissolve and react with the dimethylamine. The exact physicochemical phenomena for this process are not known. The reaction consists of a parallel-series reaction in which the dimethylamine reacts with the dissolved API feed to form the desired intermediate (C), which in turn reacts with the active feed (A) to form a dimeric by-product (D) in parallel:

$$\begin{aligned} A + B &\rightarrow C \quad \text{Main reaction} \\ A + C &\rightarrow D \quad \text{Subreaction} \end{aligned} \tag{21}$$

D is very difficult to remove in the downstream purification stages. The model assumes intrinsic first order reaction kinetics. An initial rate limiting period due to the dissolution of solids (B) was observed to be independent of solvent concentration and agitation speed within the range of conditions approved. A crude approximation of first order kinetics is assumed in the model for this dissolution controlled period. This period was observed to last until approximately 55% conversion of A for all the conditions considered, at which point the reaction appeared to be limited by the intrinsic reaction kinetics.

The kinetic model was integrated with a standard semibatch reactor model with constant volume addition (of reagent B). Consideration of the cooling capacity of the reactor resulted in a limiting relationship between the operating policy variables of feed B addition time, t_{add}, and isothermal temperature, T_{iso}. For the purposes of this study, this relationship is well-approximated with T_{iso} as a quadratic function of t_{add} since data regarding the energy balance is unavailable. The model equations used to describe this process are given in Johnson (2002).

4.5.3.1 Nominal Optimization

Sano et al. (1998) state that one of the objectives for the development of the model was to help determine the best operating conditions for maximum product yield, Y_C.

A reaction time, t_f, of less than 8 h (terminated when the rate of conversion of A falls below 0.1%) and a final yield in the impurity, Y_D, of below 2% must be maintained. The optimization problem is:

$$\max_{T_{iso}, t_{add}} Y_C \tag{22}$$

subject to:

batch reactor model equations

$$\begin{aligned} & t_f \leq 8 \\ & Y_D \leq 2\% \\ & 288 \leq T_{iso} \leq 313 \\ & 0.5 \leq t_{add} \leq 3.0 \end{aligned} \tag{23}$$

$$T_{iso} \geq 7.06(t_{add})^2 - 43.50(t_{add}) + 352.67$$

The optimal results the authors determined through repeated simulation of their model are given in Table 4.4. Optimization of an equivalent model for maximum product yield subject to the stated constraints using a nonlinear constrained Sequential Quadratic Programming (SQP) optimization software, are shown to compare reasonably well (Table 4.4).

4.5.3.2

Consideration of Uncertainty in the Stochastic Model

Uncertainty in the model parameters could have a large effect on any results predicted by the model. This may be of particular importance regarding the optimal operating policy determined subject to the safety constraint and the desired limits on process performance.

The uncertain parameters which have a nonnegligible influence on yield of C, Y_C, yield of D, Y_D and the final time, t_f, are the kinetic rate law parameters, the transition point from dissolution controlled kinetics to intrinsically controlled kinetics, X_{diss}, and the isothermal temperature, T_{iso}. These parameters are assumed to be uncorrelated.

The main results from sensitivity analysis of the sample generated under the SQP nominal optimum conditions are shown in Table 4.5. The results indicate that the

Table 4.4 Comparison between the optimal literature results (determined through repeated simulation) and optimal results obtained with SQP optimization.

		Sano et al. (1998)	SQP optimization
Criteria	Y_C(%)	Not given	97.1
	Y_D (%)	~1	1.4
	t_f (h)	~7	6.7
Operating policy	T_{iso} (K)	298.0	296.8
	t_{add} (h)	1.7	1.79

Table 4.5 Key standardized regression coefficient contributors to predicted uncertainty under the nominal optimum operating policy.

	Yield C	Yield D	Final time
Ea_1	−0.62	0.60	0.99
A_1	0.02	−0.02	−0.03
Ea_2	0.74	−0.76	0.03
A_2	−0.03	0.03	−0.00

activation energy parameters in the intrinsic reaction rate laws (Ea_1 and Ea_2) are the most strongly related to the observed uncertainty in the output criteria.

The optimization problem under uncertainty aims to maximize the expected product yield (Y_C) with the expected violation in both the impurity yield (Y_D) and the final time (t_f). The formulation of the stochastic optimization problem is:

$$\max_{T_{iso}, t_{add}} F\big(E\{\Phi\}\big) = 1 - \big\{w_1 E\{Y_C\} - w_2 E_{viol}\{Y_D \leq 2.0\} - w_3 E_{viol}\{t_f \leq 8.0\}\big\} \qquad (24)$$

subject to the process model equations with stochastic parameters.

The operating policy decisions, t_{add} and T_{iso}, are scenario independent, assuming the *a priori* here and now mode of control where knowledge of particular realizations of the uncertainties is not assumed in the optimal solution. One-sided stochastic constraints are incorporated to maintain the desired limitations on the impurity yield (Y_D less than 2.0%) and the final time (t_f less than 8 h). Since certain realizations within the uncertainty space may result in values of the endpoint impurity yield and final time exceeding the desired limits, expected violations of these limits of 1.5% and 1 h, respectively, are permitted. This allows some tolerance to the desired limits (E_{viol} the summed extent of violation of those observations failing divided by the total number of observations), which permits the determination of optimal solutions which are not overly conservative.

A stochastic optimization algorithm is used to solve the problem, where a Hammersley sequence sampling scheme is used to place observations in the uncertainty space. A reduced convergence criterion of ±2% deviation in the output distribution parameters is permitted to reduce the number of observations per objective function evaluation.

The results for the optimizations under uncertainty in the key parameters are given in Table 4.6, where the value for the product yield objective mean-variance weight (κ) is 0.5. It is clear that under the nominal optimal operating policy decisions, the expected violation of the final time, $E_{viol}\{t_f\}$, is significantly greater (4.49 h) than the desired limit (1 h). In addition, the expected yield of impurity, $E\{Y_D\}$ at 2.75% with an expected violation, $E_{viol}\{Y_D\}$, of 1.39% is not satisfactory.

Comparing the results obtained when uncertainty was considered, shown in Table 4.6, it can be immediately seen that an improvement in the Y_C mean-variance objective is achieved (largely due to the 47% reduction in the variance) with maintenance of both the stochastic constraints for $E_{viol}\{t_f\}$ and $E_{viol}\{Y_D\}$. Huge reductions in the both the expected final time (2.35 h) and the 5–95% fractile width (5.17 h) are

Table 4.6 Validated process optimization results under uncertainty.

Criteria	Nominal optimal operation	Uncertain optimal operation
Scenarios	456	418
Mean-variance $\{Y_C\}$	0	0.234
$[E\{Y_C\}$ (%), $Var\{Y_C\}]$	[94.35, 50.4]	[94.30, 26.9]
$E\{Y_D\}$ (%)	2.75	2.77
$E\{t_f\}$ (h)	9.34	2.35
$FW\{Y_C\}$ (%)	18.73	15.92
$FW\{Y_D\}$ (%)	8.83	7.55
$FW\{t_f\}$ (h)	24.97	5.17
$[Pr_{pass}\{Y_D \leq 2.0\}, Pr_{pass}\{t_f \leq 8.0\}]$	[0.59, 0.59]	[0.53, 0.98]
$[E_{viol}\{Y_D \leq 2.0\}, E_{viol}\{t_f \leq 8.0\}]$	[1.39, 4.49]	[1.25, 0.05]
Decisions		
t_{add} (h)	1.79	1.12
T_{iso} (K)	296.8	312.4

observed, with no significant loss in the expected product yield or increase in the impurity yield. Full statistical information can be obtained from the results of the stochastic optimization (Johnson and Bogle 2006).

The use of this approach allows the designers to explore the effects of uncertain parameters on the design of unit operations, and of whole processes (Johnson 2002). In spite of the considerable computational time required this can be achieved with relatively simple models. The approach can also highlight which parameters are the most sensitive to the design and therefore may require better prediction or measurement to be able to have confidence in the design.

4.5.4
Case Study 4: Biochemical Process Design

Much biochemical process development is done using simple tools such as BioPro-designer (Petrides 1994). This tool accounts for material and energy flows and in particular is useful in tracking the large amounts of water that are used. However the incorporation of detailed models for fermentation is difficult particularly if structured models are used where the organism which produces the product organism is modeled with different compartments inside the cell. This is necessary if there are separate phases in the cell as is the situation in this case study where the product forms as a solid granule or inclusion body (IB) inside the cell. In order to optimize the process it is necessary to consider this solid phase since it will significantly affect the primary separation.

Biochemical processes and some batch chemical plants consist of cascades of complex unit operations, which process a physical stream to produce valuable products.

The product is produced in a fermenter, which is usually designed to maximize the biological yield of product. However, it is not always true that maximal biochemical yield will necessarily produce the most efficient yield of purified product since effective separation also depends on the production of by-products that must be separated, and also sometimes on the physical form of the product. To consider these aspects it is again necessary to consider the fermenter design in tandem with the rest of the process. This can only be done effectively with CAPE tools. In this case study the product forms as an inclusion body within the cells so the physical form of the product affects the efficiency of the process. The models must include the size of the inclusion bodies as they grow and are separated and so this study includes population balance techniques for modeling particle size.

The process produces a protein which forms as inclusion bodies in recombinant *E. coli* cells in a fermenter operated in fed-batch mode and purified by a chain of downstream processing units (Bogle, Hounslow and Middelberg 1991). This process is typical for the production of animal hormones such as bovine somatotropin (BST) and porcine somatotropin (pST), for which much of this work was done, and for synthetic insulin. A culture of genetically engineered cells is fully grown in a fermenter in a solution of various salts using glucose as a carbon source. After initial growth phase the *E. coli* cells are induced either chemically or thermally after which the protein is produced and grows as inclusion bodies within the cell. The inclusion bodies continue to grow in size until the cell population is killed by raising the temperature yielding a slurry of cells each containing an inclusion body.

Once the fermentation has been stopped the cells within the broth must be concentrated in a filtration stage, in which some of the water is removed, and the cells disrupted in a high pressure homogenizer to release the intracellular material which includes the solid inclusion bodies. The homogenate is then diluted with water to improve its handling characteristics prior to centrifugation. In the centrifuge the dense inclusion bodies are collected as the concentrate while the less dense cell debris is lost in the supernatant. Naturally, some inclusion bodies are lost and some debris will appear in the concentrate. Further purification stages are required prior to final formulation.

The optimal operating conditions for a plant will depend on the characteristics of the product, in particular number and size of inclusion bodies. These characteristics can be measured after a fermentation and this information used to decide optimal conditions. Simulations can be used to determine timings for key events for optimal operation (Bogle et al. 1995). Here we investigate the optimization of the process given a known set of fermenter outlet conditions.

4.5.4.1 The Optimization Problem

A key tradeoff occurs in this process: inclusion body recovery and product purity vary in a conflicting manner when using the operation of the centrifuge as a manipulated variable to improve performance (see Fig. 4.11). This results in an optimization problem: only one of the objectives can be optimized at a time with the manipulation of the centrifuge variables yielding low values for the other objectives. This indicates

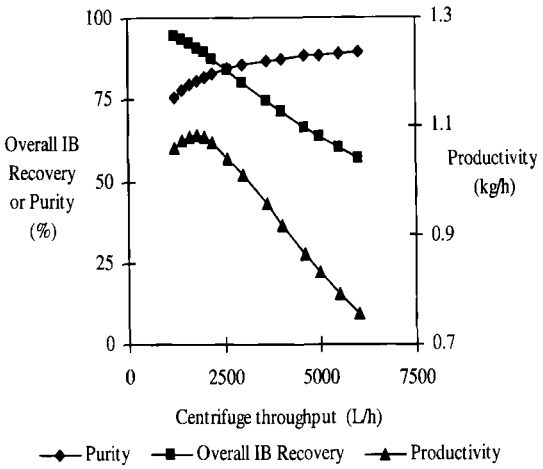

Figure 4.11 Tradeoffs between product purity, recovery and productivity as a function of one operating variable-centrifuge throughput.

that no *overall* process optimum with acceptable values for each objective can be attained with these specified variables, although both are of practical importance. However, it is important that process interactions are not to be neglected when an overall process optimum is intended, and it is of particular interest to ensure that acceptable levels of recovery, purity, and productivity can be achieved when the entire process is considered simultaneously The objectives can be optimized separately or the whole process can be considered and all values of the objectives examined. The objective functions for the optimization of the BST production process are IB recovery, product purity, and process productivity. The time invariant parameters and control variables and their limits are described in the next section. More details can be found in Graf (1996).

In this work we chose to focus on the following operational case: a fermentation has taken place and an engineer wishes to determine the best operating conditions economically. The fermentation time was fixed at 14 h. The boundaries of the optimization variables are either due to practical limitations, e.g., for the settling area and the throughputs, or due to the lack of further experimental data, e.g., for the number of homogenizer passes.

4.5.4.2
Maximization of the Inclusion Body Recovery

The results of the optimization of the overall inclusion body recovery are given in Table 4.7. The results show that a maximum of 95% of all inclusion bodies can be recovered by manipulating the specified variables. The results from the simulation (Fig. 4.11) show the contrasting behavior of IB recovery and purity when variables influence the separator-centrifuge efficiency. This feature is supported by the optimization results. The purity is low with 73.8% when the IB recovery is optimized. A productivity of 1.021 kg BST h^{-1} can be achieved due to the high recovered mass of product. Each optimization variable has taken the value of one of its limits except the separator-centrifuge settling area. It has been found during the simulation that the

Table 4.7 Results for the maximization of the IB recovery. The table shows the values of the objectives and the optimization variables determined for the maximum.

Overall IB recovery (%)	Purity (%)	Productivity (kg BST h^{-1})	Overall process time (h)	Final process volume (L)	Recovered mass of BST (kg)
95	73.8	1.021	37.3	1304	38.1

Harvester settling area (m^2)	Harvester throughput (L h^{-1})	Number of passes (–)	Dilution rate (–)	Separator settling area (m^2)	Separator throughput (L h^{-1})
250000	1200	3	4	105837	1200

IB recovery increases with the number of homogenizer passes and a higher dilution rate. The upper limits of these variables are thus the expected values. The IB recovery is maximized when the losses in the centrifuges are minimized suggesting that the settling areas should take the values of the upper limits and the throughputs of the lower limits. In the case of the separator-centrifuge settling area, the critical IB separation diameter is already so small that an increase of the settling area cannot influence the IB recovery any more, an effect which is based on the discretization of the IB size distribution: the critical IB separation diameter is already smaller than the smallest diameter of the discretized IB size distribution. Hence the rate of change of the IB recovery with the further increase of the settling area has fallen below the sensitivity of the gOPT optimization procedure, and the optimization has stopped, showing values for the separator-centrifuge settling area which are not bounds. However, an IB recovery of 100% could not be achieved due to losses in the first centrifuge and the nonideal separation efficiencies.

4.5.4.3

Maximization of the Product Purity

The values of the objectives and the optimization variables for maximizing the product purity are listed in Table 4.8. A product purity of 92.1% in the separator-centrifuge sediment can be achieved with a concomitant low overall IB recovery of 12.7%, and a productivity of 0.163 kg BST h^{-1}. These results prove again the main feature of this type of process: the higher the purity, the lower the IB recovery and productivity. The values of the optimization variables show that the loss of cells in the harvester-centrifuge is minimized by the highest possible settling area and the lowest throughput. Three homogenizer passes and a dilution rate of 1.1 are expected values from the simulation whereas the values for the separator-centrifuge are not on the bounds. As has been earlier found with the discretized IB size distribution, any further change of the separator-centrifuge settling area and the throughput would not increase the purity, since the critical diameter for cell debris is already bigger than the biggest discretized diameter of the cell debris size distribution.

Table 4.8 Results for the maximization of the purity. The table shows the values of the objectives and the optimization variables determined for the maximum.

Overall IB recovery (%)	Purity (%)	Productivity (kg BST h^{-1})	Overall process time (h)	Final process volume (L)	Recovered mass of BST (kg)
12.7	92.1	0.163	30.6	366	5.1

Harvester settling area (m^2)	Harvester throughput (L h^{-1})	Number of passes (–)	Dilution rate (–)	Separator settling area (m^2)	Separator throughput (L h^{-1})
250000	1200	3	1.1	92062	3203

4.5.4.4

Maximization of the Process Productivity

Table 4.9 shows the results for maximizing the productivity. In this optimization, an overall productivity of 1.16 kg BST and recovery of 93.5% is yielded whereas the purity is low at 55.7%. Again, the discrepancy between the IB recovery, productivity, and the purity is demonstrated: a high productivity and recovery together with a low purity.

These results clearly prove that only one objective can be maximized at a time using the specified variables. The settling areas of both centrifuges are pushed to the upper bounds. This is expected since the best recovery of IBs will increase the productivity, and the settling areas do not influence the overall processing time. Furthermore, the throughput of the first centrifuge is 1200 L h^{-1} due to the best cell and thus IB recovery. The values for the harvester-centrifuge settling area and its throughput have been the same for all three maximizations suggesting that the influence of the

Table 4.9 Results for the maximization of the productivity. The table shows the values of the objectives and the optimization variables determined for the maximum.

Overall IB recovery (%)	Purity (%)	Productivity (kg BST h^{-1})	Overall process time (h)	Final process volume (L)	Recovered mass of BST (kg)
93.5	55.7	1.16	32.7	815	37.9

Harvester settling area (m^2)	Harvester throughput (L h^{-1})	Number of passes (–)	Dilution rate (–)	Separator settling area (m^2)	Separator throughput (L h^{-1})
250000	1200	2	2.5	250000	1811

harvester-centrifuge on the objectives is negligible as long as its efficiency is maximized. The values for the number of homogenizer passes, the dilution rate, and the separator-centrifuge throughput are the values previously found as suboptimal for the productivity and were thus expected.

The objectives IB recovery, purity, and productivity have been maximized separately. A maximum IB recovery of 95%, a purity of 92.1%, and a productivity of 1.16 kg BST h^{-1} processing time can be achieved in separate optimizations of the specified variables. The optimization results confirm the previously found feature of this type of biochemical process: the contrasting behavior of IB recovery and purity. It has been demonstrated that only one of these objectives can be optimized with concomitant low values of the other objectives when operational and design variables are used. We have found that higher levels of each objective can be found if structural changes are made, in particular by adding a recycle around the centrifuge. An acceptable compromise has thus been found for high values of the objectives.

These results have been obtained assuming a set of experimental data from one of many fermentations undertaken. To achieve the best process design the ideal would be to operate the fermenter in such a way as to allow the inclusion bodies to grow as much as possible and then obtain the cleanest split possible between inclusion bodies and cell debris. Models have been developed for the nucleation and growth of the inclusion bodies using population balance models (Graf) as well as for the growth of the host organism. These have also been implemented but a formal optimization is not valuable. It will inevitably result in requesting the arbitrary upper limit on the fermentation time since the stopping of the growth of the inclusion bodies has not been modeled and is not understood.

The unit operation and process design can be achieved by the use of CAPE tools but this case study shows how development of designs in many new areas needs to be done in close conjunction with laboratory and pilot plant. This is especially true when designs are being optimized since they seem very often to predict designs that are on the boundary which is least understood physically. This then should lead to a planned and directed new experimental program to help in understanding the key process bottlenecks.

4.5.5
Case Study 5: Design of Fluid Bed Reactor

The micro-electronic and photovoltaic (PV) industries require high-purity silicon feedstock for production of integrated circuits and solar cells. Unfortunately, the cost of producing high-purity silicon, around \$40–\$65 kg^{-1}, is too high for the photovoltaic industry. Since their silicon purity requirements are not as restrictive, PV manufacturers have so far been able to use silicon that does not meet quality specifications as feedstock for solar cell production. Yet, this source of feedstock is diminishing. The annual rate of growth of total installed capacity of PV systems varied between 20% and 40% from 1992 to 2001 (Ydstie 2004), but the growth in the electronics

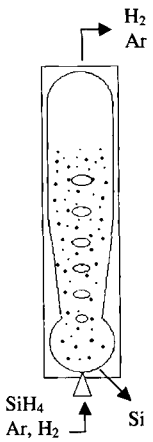

Figure 4.12 Schematic of fluid bed reactor for silane decomposition.

industry is 10% or less. Continued growth in the PV market is therefore contingent on new sources of solar-grade silicon.

A promising method of affordable solar-grade silicon production involves thermal decomposition of SiH4 (silane) inside a fluid bed reactor (Lord and Milligan 1998). A diagram of the reactor is shown in Fig. 4.12. The silane feed is preheated and delivered to the reactor in a single jet or multiple jets through the primary injector at the bottom of the reactor. A secondary injector is used to stabilize the jet. Resistance wall heaters are used to maintain reactor temperature. Hydrogen, a product of reaction, and the fluidizing gas are vented out the top. Silicon particles can be removed as product from an outlet close to the bottom of the reactor. The objective of our study is to develop a model suitable for control systems design, scale-up and process optimization.

4.5.5.1

Model Development

The fluid bed population balance model (White and Ydstie 2004) assumes that Silane decomposition in the fluid bed reactor occurs according to the overall reaction

$$SiH_4 \rightarrow Si + 2\ H_2 \tag{25}$$

The analysis of solid-phase behavior is presented first, and the new kinetic expressions are highlighted. To predict changes in silicon particle size, the model tracks particle movement to and from different intervals. This is accomplished by using mass and number balances over each size interval with constitutive equations to define particle growth. A representation of particle movement between size intervals is shown in Fig. 4.13.

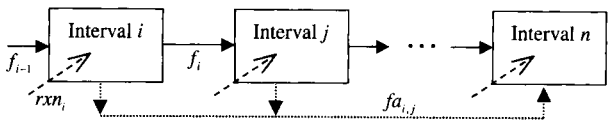

Figure 4.13 Progression of silicon particles through size intervals.

Changes in the particle size distribution can be described with a mass balance over each size interval. Ignoring the potential for particle aggregation initially allows the change in number of moles of silicon in an interval (M_i) to be defined as:

$$\frac{dM_i}{dt} = f_{i-1} - f_i + rxn_i . \tag{26}$$

So to predict the size distribution, it is necessary to define molar flow due to particle growth from one interval to the next (f_i) as well as the number of moles added to each size interval due to silane decomposition (rxn_i). This equation is then combined with a number balance and combined with rate expressions for chemical reaction. Since reaction occurs through heterogeneous and homogeneous pathways, the overall reaction rate is considered to be the sum of the rate expressions for both pathways.

$$r = r_{het} - r_{hom} \tag{27}$$

Rate expressions for both the heterogeneous and homogeneous reactions can be obtained from Furusawa et al. (1988). The reaction rate expressions require knowledge of silane and hydrogen concentrations, which can be determined from a gas phase model of the bed zone of the reactor which behaves as a CSTR so that we can write:

$$\begin{aligned} \text{silane} \quad & \frac{d(V_g \cdot C_{so})}{dt} = F_{in} \cdot C_{si} - F_{out} \cdot C_{so} - r \cdot V_g , \\ \text{hydrogen} \quad & \frac{d(V_g \cdot C_{ho})}{dt} = -F_{out} \cdot C_{ho} + 2r \cdot V_g , \end{aligned} \tag{28}$$

where V_g is the volume of gas in reactor (L); C_{so} is the concentration of silane leaving reactor (mol L^{-1}); C_{si} is the concentration of silane into reactor (mol L^{-1}); C_{ho} is the concentration of hydrogen leaving reactor (mol L^{-1}); F_{in} is the flow into reactor (L s^{-1}); and F_{out} is the flow leaving reactor (L s^{-1}).

The model has been further modified to account for particle aggregation using binary interactions so that:

$$fa_{i,j} = k_{i,j} C_i C_j \tag{29}$$

The value of $k_{i,j}$ can be estimated by comparing model predictions with experimental data. A typical model result is shown in Fig. 4.14.

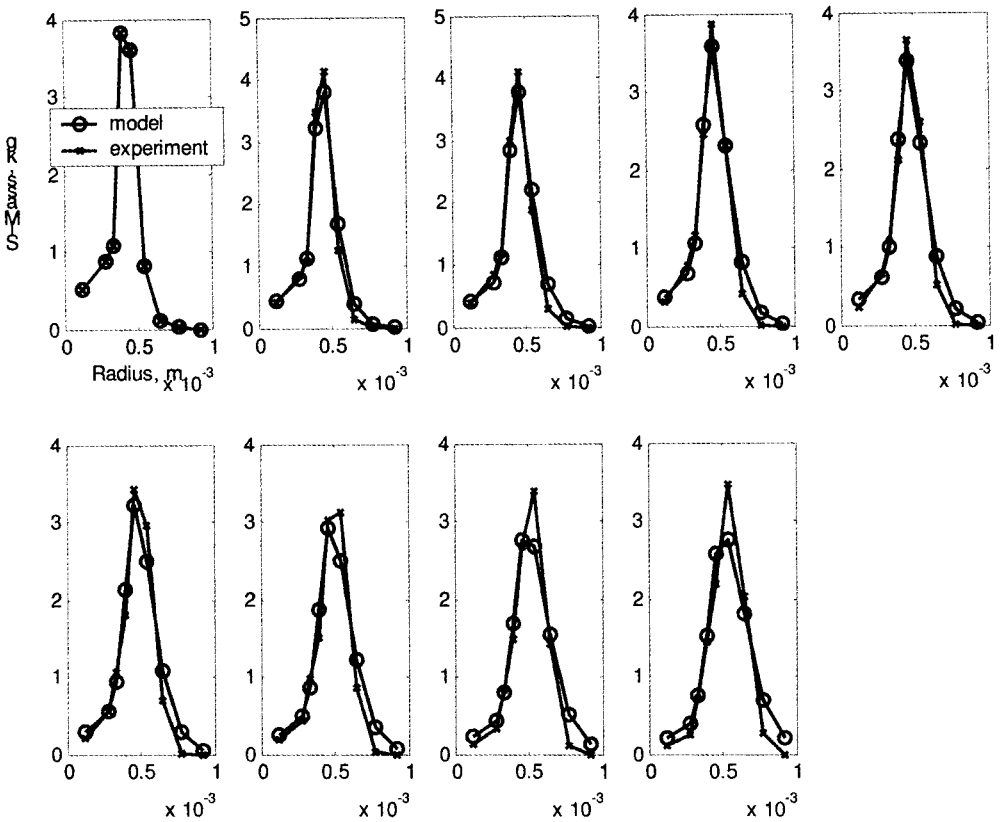

Figure 4.14 Experimental (x) and modeled (o) size distribution with no aggregation or loss of powder.

4.6 Conclusions

The five case studies have shown the way in which CAPE tools can be used to design thermodynamically and physically complex industrial units and flowsheets. Increasingly this level of detail is being demanded by designers especially where tight quality, safety and environmental requirements are being expected. In all cases there has been a clear need for sophisticated modeling tied closely to bench-scale or pilot plant experimental systems to ensure that the right data is obtained to the right degree of accuracy.

Some of this work has been done with commercial tools and some with bespoke programs. But it is clear that more sophisticated systems are required to facilitate rapid development of such models involving complex thermodynamics, irregular geometries, and particulates. These challenges remain. Systems which guarantee thermodynamic consistency are required as well, and systems incorporating the sys-

tematic and efficient assessment and minimization of uncertainty and its use to guide experiments remains a challenge to the developers of CAPE tools.

References

1 *Bogle I. D. L., Cockshott A. R., Bulmer M., Thornhill N., Gregory M.,* and *Deghani M.* (1995) A Process Systems Engineering View of Biochemical Process Operations. *Comput. Chem. Eng.* 20(6/7), 943–949.

2 *Bogle I. D. L., Hounslow M. J.,* and *Middelberg A. P. J.* (1991) Modelling of inclusion body formation for optimisation and recovery in a biochemical process. In Proceedings of 4th International Conference on Process Systems Engineering, Montebello, Canada.

3 *Bogle I. D. L.* and *Cameron D.* (2002) CAPE tools for off-line simulation, design and analysis. In *B. L. Braunschweig* and *R. A. Gani* (eds.) *Software Architectures and Tools for Computer-aided Process Engineering,* Elsevier, Amsterdam.

4 *Callen H. B.* (1985) Thermodynamics and an Introduction to Thermostatics, Wiley, New York.

5 *Eggersmann M., Hackenberg J., Marquardt W.,* and *Cameron I. T.* (2002) Applications of modelling – a case study from process design. In *B. L. Braunschweig* and *R. A. Gani* (eds.) *Software Architectures and Tools for Computer-Aided Process Engineering,* Elsevier, Amsterdam.

6 *Farschman C. A., Viswanath, K. P.,* and *Ydstie B. E.* (1998) Process Systems and Inventory Control. *AIChE J.* 44(8), 1841–1855.

7 *Frank R. A., Finn C. W.* and *Elliott J. F.* (1989) Physical Chemistry of the Carbothermic Reduction of Alumina in the Presence of a Metallic Solvent: 2. Measurements of Kinetics of Reaction. *Metall. Mater. Trans. B* 20(2), 161.

8 *Furusawa T., Kojima T.* and *Hiroha H.* (1988) Chemical Vapor Deposition and Homogeneous Nucleation in Monosilane Pyrolysis within Interparticle Spaces: Application of Fines Formation Analysis to Fluidized Bed CVD. *Chem. Eng. Sci.* 43(8), 2037–2042.

9 *Garcia-Osorio V.* and *Ydstie B. E.* (2003) Distributed, Asynchronous and Hybrid Simulation of Process Networks Using Recording Controllers. *Int. J. Robust Nonlinear Control* 14, 227–248.

10 *Garcia-Osorio V.* and *Ydstie B. E.* (2004) Vapor Recovery Reactor in Carbothermic Aluminum Production. *Chem. Eng. Sci* 59(10), 2053–2064.

11 *Gerogiorgis D. I., Ydstie B. E.* and *Seetharaman S. S.* (2002) A steady state electrothermic simulation analysis of a carbothermic reduction reactor for the production of aluminium. In *Cross M., Evans J. W.* and *Bailey C.* (eds.) *Computational Modeling of Materials, Minerals, and Metals Processing:* 273; Warrendale, PA (TMS).

12 *Gerogiorgis D. I.* and *Ydstie B. E.* (2003a) A finite element CFD sensitivity analysis for the conceptual design of a carbothermic aluminum reactor. In *Crepeau P.* (ed.), *Light Metals 2003*: 407; Warrendale, PA (TMS).

13 *Gerogiorgis D. I., et al.* (2003) Process Systems Tools for Design and Optimization of Carbothermic Reduction Processes. In *Das S. K.* (ed.) *Aluminum 2003,* Warrendale, PA (TMS) (in press).

14 *Gerogiorgis D. I.* and *Ydstie B. E.* (2003b) An MINLP model for conceptual design of a carbothermic aluminum reactor. In *Proceedings of European Symposium on Computer-Aided Process Engineering (ESCAPE-13),* Lappeeranta, Finland, pp. 131–136.

15 *Graf H.* (1996) Modelling and Optimisation of an Inclusion Body Type Biochemical Process. Externe Diplomarbeit (Universitat Dortmund) Project report, Dept of Chemical Engineering, University College, London.

16 *Graf H.* and *Bogle I. D. L.* (1997) Simulation as a tool in at-line prediction and control of biochemical processes. In *Proceedings of the 1st European Conference on Chemical Engineering,* ECCE1 Florence, Italy.

17 *Grossmann I. E., Westerberg A. W.* (2000), Research challenges in process systems engineering. *AIChE J.* 46, 1700–1703.

18 *Hagemann J., Fraga E. S.* and *Bogle I. D. L.* (2001) Distillation column design for improved exergy utilisation and its impact on closed loop performance. In *Proceedings of the World Congress of Chemical Engineering,* Melbourne, Australia, Sept 2001.

19 *Hangos K.* and *Cameron I. T.* (2001) *Process Modelling and Model Analysis.* Academic Press, New York.

20 *Ingram G. D., Cameron I. T., Hangos K. M.* (2004) Classification and Analysis of Integrating Frameworks in Multiscale Modelling. *Chem. Eng. Sci* 59(11), 2171–2187.

21 *Johansen K., et al.* (2000) Carbothermic aluminum. In *Proceedings of the Sixth International Conference on Molten Slags, Fluxes and Salts* (paper #192), Stockholm, Sweden (CD edition).

22 *Johansen K.* and *Aune J. A.* (2002) US Patent 6,440,193 to Alcoa Inc. & Elkem ASA.

23 *Johnson D. B.* (2002) Integrated design under uncertainty for pharmaceutical processes. PhD Dissertation, University of London.

24 *Johnson D. B.* and *Bogle I. D. L.* (2006) An approach for integrated design under uncertainty of pharmaceutical processes. Reliable Computing (in press).

25 *Kaibal G.* (1990) Energieintegration in der thermische verfahrenstechnik. *Chem. Ing. Tech.* 62(2), 99–106.

26 *Kaibel G., Blass E.*, and *Kohler J.* (1989) Gestaltung destillativer Trennungen unter Einbeziehung thermodynamischer Gesichtspunkte. *Chem. Ing. Tech.* 61(1), 16–25l.

27 *Kjelstrup S.* and *Hafskjold B.* (1996) Nonequilibrium molecular dynamic simulations of steady state heat and mass transport in distillation. *Ind. Eng. Chem. Res.* 35, 4203–4213.

28 *Lord S. M.* and *Milligan R. J.* (1998) Method for Silicon Deposition, US Patent 5,798,137.

29 *Luyben W.* (1990) *Process Modelling Simulation and Control for Chemical Engineers.* McGraw-Hill, Boston.

30 *Mangold M., Motz S., Gilles E. D.* (2002) Network theory for the structured modelling of chemical processes. *Chem. Eng. Sci.* 57, 4099–4116.

31 *Motzfeldt K., Kvande H., Schei A., Grjotheim K.* (1989) Carbothermal Production of Aluminum – Chemistry and Technology. Al Verlag, Dusseldorf, Germany.

32 *Oh M.* and *Pantelides C. C.* (1994) A Modelling and Simulation Language for Combined Lumped and Distributed Parameter Systems. In *Proceedings of the 5th International Conference on Process Systems Engineering*, Kyongju, Korea 1, 37–44.

33 *Petrides D. P.* (1994) Biopro designer – an advanced computing environment for modelling and design of integrated biochemical processes. *Comput. Chem. Eng.* 18, S621–S625.

34 *Ratkje S. K. E., Hansen E. M., Lien K. M.* and *Hafskjold B.* (1995) Analysis of entropy production rates for design of distillation columns. *Ind. Eng. Chem. Res.* 34(9), 3001–3007.

35 *Sano T., Sugaya T.* and *Kasai M.* (1998) Process improvement in the production of a pharmaceutical intermediate using a reaction calorimeter for studies of the fraction kinetics of amination of a bromopropyl compound. *Organic Res. Develop.* 2, 169–174.

36 *Sauar E., Ratkje S. K.* and *Lien K. M.* (1996) Equipartition of forces – a new principle for process design and optimization. Ind. *Eng. Chem. Res.* 35(11), 4147–4153.

37 *Sauar E., Rivero R., Kjelstrup S.* and *Lien K. M.* (1997) Diabatic column optimization compared to isoforce columns. *Energy Conserv. Mgmt.* 38(15), 1777–1783.

38 *Sauar E.* and *Ydstie B. E.* (1998) The temperatures of the maximum reaction rate and their relation to the equilibrium temperatures. *J. Phys. Chem. A* 102, 8860–8864.

39 *Skogestad S.* (1997) Dynamics and control of distillation columns. *Trans. IChemE Part A* 75, 539–562.

40 *Swaney R. E.* and *Grossmann I. E.* (1985) An index for operational flexibility in chemical process design. Part 1 Formulation and theory. *AIChE J.* 31(4), 621–630.

41 *Tondeur D.* and *Kvaalen E.* (1987) Equipartition of entropy production – an optimality criterion for transfer and separation processes. *Ind. Eng. Chem. Res.* 26(1), 50–56.

42 *White C.* and *Ydstie B. E.* (2004) Modeling the Fluid Decomposition of Silane to form Photovoltaic Grade Silicon in a Fluid Bed Reactor, Technical Report, Carnegie Mellon, Chemical Engineering.

43 *Ydstie B. E.* (2004) Decision making in complex organizations: the Adaptive Enterprise. *Comput. Chem. Eng.* (in press).